Linear dynamic range of a Rydberg-atom microwave superheterodyne receiver

Fengchuan Wu ⬤, Qiang An,[*] Zhanshan Sun, and Yunqi Fu

College of Electronic Science and Engineering, National University of Defense Technology, Changsha 410073, China

In recent years, electric field measurement techniques based on Rydberg atoms have shown unique advantages in high sensitivity and wideband applications and miniaturization. The Rydberg atom receiver senses the electromagnetic signal using the quantum coherence effect, which overcomes the inherent defects of traditional electronic receivers in terms of thermal noise, insertion loss of microwave devices, and the use of wavelength-dependent antennas, thus providing the Rydberg atomic receivers the potential to become the next generation of microwave receivers. For some particular application scenarios such as radar and communication, superheterodyne reception is a critical technical approach, and the linear dynamic range is an essential factor in evaluating the performance of the superheterodyne receivers. It is challenging to promote the Rydberg atomic receiver without figuring out the influence of system parameters on the linear dynamic range. This paper starts with the response mechanism of the Rydberg atomic superheterodyne receiver, and a theoretical model is established to simulate the atom-microwave responses. Then the harmonics' generation mechanism is discussed, and the atomic linear dynamic range under different probe light Rabi frequencies is studied further. Furthermore, a method to evaluate the antiblocking performance of the system is proposed. This work is expected to provide theoretical guidance for the design and performance optimization of the Rydberg atomic superheterodyne receiver.

I. INTRODUCTION

In recent years, with the further development of quantum microwave measurement technology, Rydberg atoms' electromagnetic-induced transparency (EIT) effect has attracted much attention in microwave applications. The Rydberg atom can construct a superheterodyne receiver by locking laser frequencies and adding a microwave local oscillator (LO) signal. It has been studied in amplitude modulation (AM), frequency modulation (FM), quad phase shift keyed (QPSK), quadrature amplitude modulation (QAM), and other modulated signal reception [1–6], spectrum analysis [7], the direction of arrival estimation [8], pulse ranging [9], and other applications. Compared with traditional electronic antennas, one of the advantages of using Rydberg atoms is that the responsiveness is independent of the sensor size, which can break through the limitation of the Chu limit [10–15]. Second, the Rydberg atom has an ultra-wideband working band, which can theoretically realize the responsibility of the electric field in the ultralow to infrared frequency band [7,16–18]. Without changing the hardware, the electric field frequency response to the Rydberg atom can be changed by tuning the laser frequency. In addition, the Rydberg atomic sensor can achieve sensitivity on the order of $\mu V\,m^{-1}\,Hz^{-1/2}$ [19–26], which is better than the traditional electronic receivers. Furthermore, there is no metal structure in the sensor, and the EIT effect of the Rydberg atom does not respond to the space electric field by strongly absorbing the space electromagnetic wave energy. Therefore, this kind of sensor has little disturbance on

the electric field to be measured, which can achieve all-optical nondestructive detection [27,28]. Consequently, the study of electromagnetic resonance structures has emerged to improve the electric field sensitivity of the Rydberg atomic receiver [29–31]. Based on the in-depth study of the physical response mechanism of the Rydberg atom superheterodyne reception [32–40], the complete Rydberg atom superheterodyne reception link model can be established [41]. Hence, the Rydberg atom has excellent potential as a new generation of wireless receivers.

In a superheterodyne receiving system, linear dynamic range (LDR) also plays a decisive role in receiving system performance besides sensitivity. However, it has yet to be thoroughly discussed in current research. LDR refers to the strength range of the input signal that enables the receiver to detect the received signal without distortion. When the superheterodyne receiver with poor linear response characteristics receives a strong signal, it will show prominent high-order harmonic components, usually considered interference in the receiving system. They can be filtered by adding a low-pass filter in the subsequent electronic information-processing module. However, when the microwave signal under test (MSUT) is a modulated signal with a specific bandwidth, the frequency bands of the harmonic components may overlap with that of the valid intermediate frequency signal (VIFS), and the harmonic components cannot be filtered. Therefore, the design of LDR is crucial. Also, the antiblocking performance is decided by LDR, and its evaluation method has yet to be thoroughly discussed. When space interference signals in the operating frequency band enter the receiver, in addition to distorting the received signal, they may also cause saturation of the receiver, blocking the reception of MSUT. Therefore,

─────────
[*]Corresponding author: anqiang18@nudt.edu.cn

if the LDR is small or the antiblocking performance is poor, it is challenging to popularize the application scenario of the Rydberg atomic microwave superheterodyne receiver.

The work of this paper is arranged into the following parts: in Sec. II the principle of the Rydberg atomic superheterodyne receiver is briefly described, and the theoretical analysis model is established by introducing the atomic linear expansion coefficient (ALEC). In Sec. III the line shape of the Rydberg atom's EIT-AT (Autler-Townes) spectrum by adjusting the incident probe light Rabi frequency is discussed first. Then the harmonics' generation mechanism and the linear response characteristic are analyzed through the transmittance spectral line shape. Finally, the LDR under different probe Rabi frequencies is analyzed in cold and thermal atomic models. In Sec. IV the influence of the interference signal on VIFS is studied. A method to evaluate the antiblocking probability is promoted, and the antiblocking performance under different probe light Rabi frequencies is discussed. The work in this paper is summarized in Sec. V.

II. PRINCIPLE OF RYDBERG ATOMIC SUPERHETERODYNE RECEIVER

The Rydberg atom is usually prepared by two-photon transition excitation. Cesium atoms are used to prepare Rydberg atoms in this work. The four-level scheme is $6S_{1/2} \rightarrow 6P_{3/2} \rightarrow nD_{5/2} \rightarrow (n+1)P_{3/2}$ ($n \geqslant 15$), which is shown in Fig. 1(a). The probe light with a wavelength of $\lambda_p = 852$ nm and Rabi frequency Ω_p excites the cesium atom from the ground state $|1\rangle$ to the intermediate excited state $|2\rangle$; the frequency of the probe light is at the transition frequency between energy levels $|1\rangle$ and $|2\rangle$ throughout. Then the coupling light with a wavelength of $\lambda_c = 510$ nm and Rabi frequency Ω_c enables the transition from the intermediate excited state $|2\rangle$ to the Rydberg state $|3\rangle$ and simultaneously enhances the transmissivity of the probe light from atomic vapor. $\Delta_c(\Delta_p)$ is the detuning of the coupling (probe) light deviating from transition frequency between state $|2\rangle(|1\rangle)$ and $|3\rangle(|2\rangle)$, and the EIT peak can be observed by scanning Δ_c or Δ_p. Then a microwave field with Rabi frequency Ω_{MW} is added to couple the Rydberg state $|3\rangle$ and $|4\rangle$, and the single EIT peak splits into two peaks, resulting in AT splitting; in this scheme, the microwave frequency is at transition frequency between state $|1\rangle$ and $|2\rangle$ throughout.

While scanning Δ_c, according to the semiclassical theory of quantum optics [37], the theoretical results of EIT spectra under different electric field intensities E are calculated, as shown in the series of curves with double peaks in Fig. 1(b). The distance between the two peaks is the Rabi frequency Ω_{MW} of the microwave field, which increases with the microwave strength E. The relationship between Ω_{MW} and E can be expressed as

$$\Omega_{MW} = \frac{\mu_{MW}E}{\hbar}, \qquad (1)$$

where $\hbar$ is the reduced Planck constant, and μ_{MW} is the transition dipole moment of the microwave field.

When the coupling light frequency is locked at the transition frequency between state $|2\rangle$ and $|3\rangle$ [$\Delta_c = 0$, shown as the vertical dashed black line in Fig. 1(b)], the relationship curve
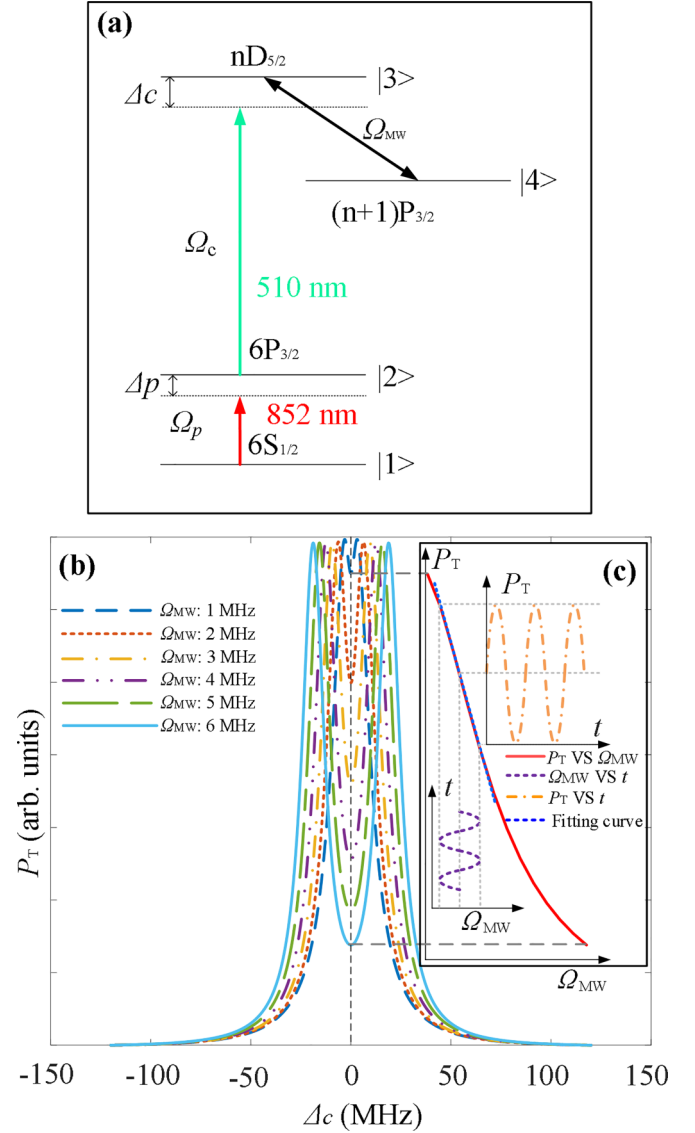

FIG. 1. (a) The Rydberg atomic four-level system; (b) EIT spectra obtained by scanning Δ_c under different Ω_{MW}; (c) the relationship curve between P_T and Ω_{MW} (solid red line) at $\Delta_c = 0$, and the dotted blue line is the linear fitting result of the solid red line. When Ω_{MW} changes with time t (dotted purple line), the relationship of P_T and t (dotted orange line) can be obtained through the red solid line mapping.

(solid red line) between the transmission probe light power P_T and the microwave Rabi frequency Ω_{MW} can be obtained, as shown by the solid red line in Fig. 1(c). The dotted blue line is the linear fitting result of the solid red line. According to the Beer-Lambert law, the expression of the solid red curve is

$$P_T = P_i e^{-P_p L C_0 \, \text{Im}[\rho_{21}]}, \qquad (2)$$

where P_i is the incident probe light power, $k_p = 2\pi/\lambda_P$ is the wave number of the probe light, and L is the propagation distance of the probe light in the atomic vapor. $C_0 = -2N_0\mu_p^2/(\varepsilon_0\hbar\Omega_p)$ is the constant determined by the system, where N_0 is the total atomic number density, $\mu_p = -2.58a_0q$ is the transition dipole moment between states $|1\rangle$ and $|2\rangle$

($a_0 = 5.3 \times 10^{-11}$ m is the Bohr radius, and $q = 1.6 \times 10^{-19}$ C is the unit charge), and $\varepsilon_0 = 8.854 \times 10^{-12}$ F/m is the vacuum dielectric constant. Im[ρ_{21}] is the imaginary part of the density matrix element ρ_{21} and can be expressed as [25]

$$\rho_{21} = \frac{-i\gamma_2|\Omega_{MW}|^2\Omega_p}{\gamma_2^2|\Omega_{MW}|^2 + 2\Omega_p^2(\Omega_c^2 + |\Omega_{MW}|^2 + \Omega_p^2)}, \qquad (3)$$

where γ_2 is the decay rate from $6S_{1/2}$ to $6P_{3/2}$. It can be seen in Fig. 1(c) that P_T decreases with the increase of Ω_{MW}. In the interval in which the dotted blue line coincides with the solid red line (the microwave Rabi frequency range corresponding to this condition is defined as the linear interval in this work), P_T has a linear relationship with Ω_{MW}. When Ω_{MW} is too small or too large, the relationship between Ω_{MW} and P_T will be nonlinear.

On the other hand, suppose there are microwave LO signal E_{LO} and MSUT E_s in free space. The time domain expressions of their electric field are expressed as

$$E_{LO} = A_{LO}\cos(2\pi f_{LO}t + \varphi_{LO}), \qquad (4)$$

$$E_s = A_s\cos(2\pi f_s t + \varphi_s), \qquad (5)$$

where A_{LO} and A_s are the electric field strengths of E_{LO} and E_s, respectively. f_{LO} and f_s represent the frequencies of E_{LO} and E_s while φ_{LO} and φ_s are phases of E_{LO} and E_s. The superposition field E_{MW} can be expressed as follows (the derivation details are given in the Appendix):

$$
\begin{aligned}
E_{MW} &= E_{LO} + E_s \\
&= \sqrt{A_{LO}^2 + B^2 + 2A_{LO}A_s\cos(2\pi\Delta f_1 t + \Delta\varphi)}\cos(2\pi f_{LO}t + \varphi_{LO}) \\
&= \left[A_{LO}\left(1 + \tfrac{1}{2}x^2\right) + A_{LO}x\cos(2\pi\Delta f_1 t) - \tfrac{1}{2}A_{LO}x^2\cos^2(2\pi\Delta f_1 t) + O(x)^3\right]\cos(2\pi f_{LO}t + \varphi_{LO}),
\end{aligned} \qquad (6)
$$

where $x = A_s/A_{LO}$, $\Delta\varphi_1 = \varphi_{LO} - \varphi_s$, and $\Delta f_1 = f_{LO} - f_s$; the nonlinear response of the Rydberg atom to the superposition field E_{MW} can be equivalent to envelop detection. When $x \ll 1$, the main frequency component of the superposition field envelope is Δf_1, and the higher harmonic component can be ignored. Substitute (6) into (1), and the relationship curve between Ω_{MW} and time t can be obtained, as shown by the dashed purple line in the rectangular coordinate system in Fig. 1(c). When $x \ll 1$, Ω_{MW} can be expressed as

$$
\begin{aligned}
\Omega_{MW} &\approx \frac{\mu_{MW}A_{LO} + A_s\cos(\Delta f_1 t + \Delta\varphi_1)}{\hbar} \\
&= \Omega_{DC} + \Omega_{AC},
\end{aligned} \qquad (7)
$$

where Ω_{DC} and Ω_{AC} contain the electric field strength information of E_{LO} and E_s, respectively, and their expressions are shown as

$$\Omega_{DC} = \frac{\mu_{MW}A_{LO}}{2\pi\hbar}, \qquad (8)$$

$$\Omega_{AC} = \frac{\mu_{MW}A_{LO}\cos(\Delta f_1 t + \Delta\varphi_1)}{2\pi\hbar}. \qquad (9)$$

Substitute (6), (1), and (3) into (2), and the relationship between P_T and t can be obtained, as shown by the dashed orange line in Fig. 1(c). When Ω_{MW} is in the linear interval. The relationship between P_T and Ω_{DC} and Ω_{AC} can be expressed as

$$P_T = P_{TDC} + P_{TAC} = a\Omega_{DC} + \kappa\Omega_{AC}, \qquad (10)$$

where $\kappa(a)$ is the ratio of the AC (DC) component of the transmitted probe light power P_{TAC} (P_{TDC}) to Ω_{AC} (Ω_{DC}), and $|\kappa|$ can be defined as ALEC, which describes the variation rate of P_{TAC} with Ω_{AC} [25]. To keep Ω_{MW} in the linear interval, Ω_{DC} should be carefully selected and one should keep $x \ll 1$. Therefore, $|\kappa|$ can be regarded as constantly equal to ALEC. According to (10), the greater the value of $|\kappa|$, the stronger responsiveness of the Rydberg atom to the weak microwave electric field, and thus the better sensitivity performance.

III. OPTIMAL ALEC AND THE LINEAR RESPONSE CHARACTERISTIC

Optimal ALEC determines the response ability of the Rydberg atom to the weak electric field signal, and the linear response characteristic determines the signal fidelity when detecting MSUT. Optimal ALEC and the linear response characteristics can be analyzed by the relationship curve of Ω_{MW} and P_T, and the EIT spectrum determines the relationship curve of Ω_{MW} and P_T. Before analyzing the optimal ALEC and the linear response characteristic, the influence of Ω_p on the EIT spectrum has been analyzed, and the influences on optimal ALEC and the linear response characteristics of the Rydberg atom have been analyzed subsequently.

The EIT-AT spectra of the atomic four-level system model under different Ω_p are studied. For simplicity, we use the cold atomic model for analysis (the thermal atom model needs to consider the spectral broadening caused by the atomic thermal motion, but the analysis basis remains unchanged), and the calculated spectrum is shown in Fig. 2(a). Here $\Omega_c = 1$ MHz, $\Omega_{MW} = 40$ MHz, $N_0 = 1 \times 10^{15}$ m^{-3}, $L = 0.02$ m. Further, consider the relationship between P_i and Ω_p,

$$P_i = \frac{\pi\left(\frac{d\Omega_p\hbar}{2\mu_p}\right)^2}{2\eta}, \qquad (11)$$

where impedance of free space $\eta = 377\ \Omega$, and the $1/e^2$ diameter of the laser beam $d = 0.76$ mm; according to (11), P_i can be calculated from Ω_p. The series of EIT-AT spectra obtained by scanning Δ_c under different Ω_p are shown in Fig. 2(a). When the Rabi frequency of the probe light gradually increases, the profile height Φ of the single transmission peak increases, as the solid blue line in Fig. 2(b). Moreover,
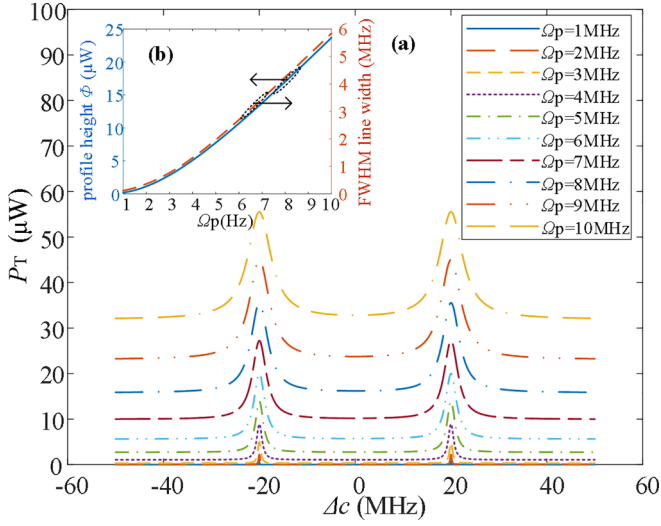
FIG. 2. (a) The EIT-AT spectra under different Ω_p; (b) the relationships of the spectral profile height (solid blue line) and the FWHM linewidth (dashed red line) vs Ω_p.

the full width half maximum (FWHM) linewidth of the single transmission peak broadens with the increase of Ω_p, as shown in the dashed red line in Fig. 2(b). Therefore, the line shape of the EIT-AT spectra can be adjusted by altering Ω_p. Similarly, fixing Ω_p and increasing Ω_c can also broaden the FWHM linewidth and raise the profile height Φ, which is not as obvious as increasing Ω_p.

A. The influence of Ω_p on optimal ALEC

The series curves of Ω_{MW} vs P_T under different Ω_p can be obtained by locking $\Delta_c = 0$, as shown in Fig. 3(a). With the increase of Ω_{MW}, P_T decreases for all curves, and there is a maximum rate $|\kappa|_{max}$ in the middle. The Rydberg atom is most
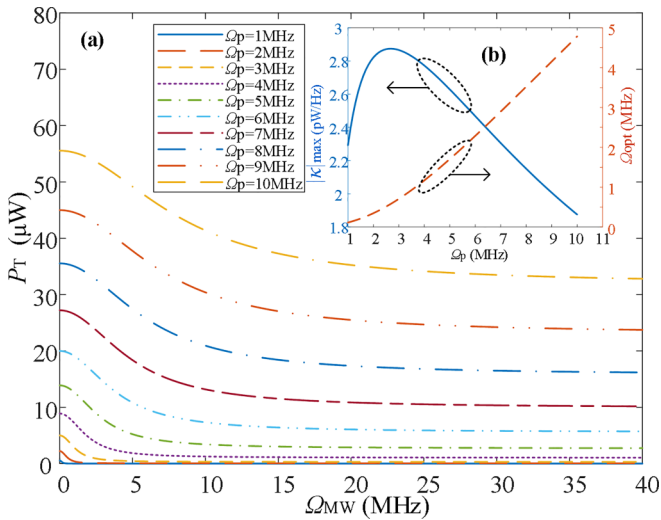

FIG. 3. (a) The relation curves of Ω_{MW} vs P_T under different Ω_p; (b) the relation curves of Ω_{opt} (dashed red line) and $|\kappa|_{max}$ (solid blue line) vs Ω_p.

sensitive to the small changes in the electric field envelope when getting $|\kappa|_{max}$.

To obtain $|\kappa|_{max}$, substitute (3) into (2) and set its second-order partial derivative result to 0, which can be expressed as

$$\frac{\partial^2 P_T}{\partial \Omega_{MW}^2} = P_i e^{-k_p L C_0 \, \text{Im}[\rho_{21}]} = 0. \quad (12)$$

By solving (12), the microwave Rabi frequency Ω_{opt}, which achieves the optimal ALEC, can be obtained. The dashed red line in Fig. 3(b) shows that Ω_{opt} is proportional to Ω_p. If we substitute (3) into (2) and find its first-order partial derivative for Ω_{MW}, and substitute Ω_{opt} into the first partial derivative, then $|\kappa|_{max}$ can be obtained. The solid blue line shows the curve of $|\kappa|_{max}$ vs Ω_p in Fig. 3(b). With the increase of Ω_p, $|\kappa|_{max}$ first increases and then decreases, with a maximum value of $|\kappa|_{max}$ between 2 MHz and 3 MHz. The broader the FWHM line width, the smaller $|\kappa|_{max}$. The higher the EIT peak's profile height, the greater the value of $|\kappa|_{max}$. When Ω_p increases from being infinitesimal gradually, the EIT spectral linewidth is not broadened significantly, while the EIT peak's profile height increases rapidly, making $|\kappa|_{max}$ increase; when Ω_p is further increased, power broadening of the EIT spectra is obvious, making $|\kappa|_{max}$ decrease.

B. The influence of Ω_p on the atomic linear response characteristic

Further, if we let $\Omega_{LO} = \Omega_{opt}$, the responsiveness of the Rydberg atom to the weak microwave electric field can be the best. Under this condition, the linear response characteristics are studied. Substitute (6), (1), and (3) into (2) to obtain the relationship between P_T and t. The relation curves of the VIFS's power spectrum density P_{TFF} and its second harmonic component P_{TSH} vs Ω_s have been obtained by performing the Fourier transform on $P_T(t)$, as shown in Figs. 4(a) and 4(b).

The curve of P_{TFF} vs Ω_s is shown in Fig. 4(a). When Ω_s is small, the Rydberg atom works in the linear interval. According to (10), P_{TFF} (P_{TAC}) is proportional to Ω_s (Ω_{AC}). When Ω_s increases to a certain extent and we keep $\Omega_{LO} = \Omega_{opt}$, Ω_{DC} shifts, and $|\kappa|$ decreases, and the increasing rate of P_{TFF} with Ω_s will be slowed. With Ω_s further increasing, $|\kappa|$ cannot be regarded as a constant, and the average value of $|\kappa|$ decreases. Thus, Ω_{MW} is outside the linear interval, and P_{TFF} decreases gradually.

On the other hand, harmonics are always present in the IF signal obtained by the Rydberg atomic superheterodyne receiver. There are two factors for harmonics generation: (1) $|\kappa|$ is not an absolute constant and varies with Ω_{MW}. The linear relationship between P_T and Ω_{MW} is not ideal. (2) The response of the Rydberg atom to the microwave electric field can be regarded as envelope detection, which is a nonlinear response. According to (6), when $x \ll 1$ is not satisfied, the second and higher harmonic components will become apparent.

The curve of P_{TSH} vs Ω_s is shown in Fig. 4(b). When Ω_s increases from being infinitesimal, P_{TSH} will become obvious gradually. With Ω_s further increasing, $|\kappa|$ changes significantly with the shift of Ω_{MW}, further deteriorating the linear response characteristics of the Rydberg atomic receiving system and promoting the growth of P_{TSH}. When Ω_s keeps
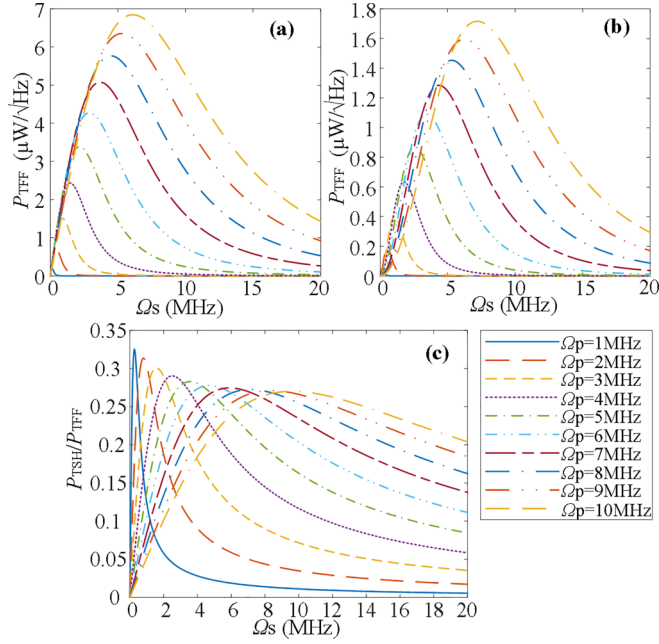
FIG. 4. The relationship curve of (a) P_{TFF}, (b) P_{TSH}, and (c) $P_{\text{TSH}}/P_{\text{TFF}}$ vs Ω_s under different Ω_p when $\Omega_{\text{LO}} = \Omega_{\text{opt}}$.

increasing and we get $\Omega_s > \Omega_{\text{LO}}$, the proportion of the second harmonic component in (6) decreases. Also, $|\kappa|$ decreases with the increase of Ω_s, and P_{TSH} decreases. Similarly, the variation of higher harmonic components with Ω_s is similar to that of P_{TSH}. In addition, with the increase of Ω_p, the spectral peak's profile height and FWHM line width increase. The maximum values of P_{TFF}, P_{TSH}, and the corresponding microwave Rabi frequency increase.

When the proportion of P_{TSH} and higher harmonic components is high, the linear response characteristics are poor, so the ratio of P_{TSH} to P_{TFF} can be used to measure the linear response characteristics of the system qualitatively. Using the calculation results in Figs. 4(a) and 4(b), a series of curves of $P_{\text{TSH}}/P_{\text{TFF}}$ vs Ω_s can be obtained under different Ω_p, as shown in Fig. 4(c). With the increase of Ω_s, the linear response characteristics deteriorate. In addition, when Ω_s takes a fixed minimum value, the linear response characteristic becomes better as Ω_p increases.

In summary, the linear response characteristics can be improved by increasing Ω_p while keeping other parameters unchanged. However, when Ω_p is large, the value of $|\kappa|_{\text{max}}$ is small, and thus the response ability of the Rydberg atom to the weak electric field signal becomes poor. Therefore, the Rydberg atomic linear response characteristics and sensitivity need to be further studied.

C. The influence of Ω_p on 1 dB compression point and the LDR

It is hard to describe the linear response characteristics of the atomic superheterodyne receiver strictly using $P_{\text{TSH}}/P_{\text{TFF}}$. In a conventional electronic receiver, the linear response characteristics can be characterized by a 1 dB compression point. A similar concept can also be constructed for the Rydberg atomic superheterodyne receiver. However, the response mechanism of Rydberg atoms to electromagnetic waves

differs from that of traditional electronic receivers. When a Rydberg atomic superheterodyne receiver responds to electromagnetic waves from space, the signal carrier is converted from microwave to probe light. For the low-noise amplifier and mixer in traditional electronic receivers, the carriers of the input and output signals are both electrical signals. Refer to the definition of the LDR of the Rydberg atomic superheterodyne receiving system in the work of the CCDC U.S. Army Research Laboratory [7]. The 1 dB compression point of the Rydberg atomic superheterodyne receiving system in 1 Hz bandwidth can be defined as the value of Ω_s or the electric field of MSUT when the power spectral density of P_{TFF} generates 1 dB compression compared to P_{linear}. When $\Omega_{\text{LO}} = \Omega_{\text{opt}}$, P_{linear} can be defined as

$$P_{\text{linear}} = |\kappa|_{\text{max}} \Omega_s. \tag{13}$$

According to the P_{TFF} obtained in Fig. 4(a), compared with (13), the relationship between the 1 dB compression point $\Omega_{1\,\text{dB}}$ of the system and Ω_p can be obtained, shown by the solid blue line in Fig. 5(a), and $\Omega_{1\,\text{dB}}$ increases with Ω_p. On the other hand, P_T also has an intensity noise, specifying its RMS (root-mean-square) amplitude P_{nf} with an approximate range from 1 to 20 pW/$\sqrt{\text{Hz}}$ [41]. Substitute P_{nf} into (13), the minimum detectable MSUT Rabi frequency Ω_{min}, and the relationship between Ω_{min} and Ω_p can be obtained, as shown by the red shaded area in Fig. 5(a). Further, the relationship between LDR and Ω_p can be obtained from $(\Omega_{1\,\text{dB}}/\Omega_{\text{min}})^2$, as shown by the blue shaded area in Fig. 5(b). With the increase of Ω_p, LDR increases, and the increase rate slows.

On the other hand, the thermal atom is widely used in the measurement, and the case of the thermal atom model is further considered. In this model, the EIT spectrum produces a variety of broadening due to the atomic thermal motion, and the most significant among various factors is the Doppler effect caused by the atomic thermal motion. The Doppler averaged ρ_{21} can be expressed as [37]

$$\rho_{21D} = \frac{1}{\sqrt{\pi} u} \int_{3u}^{3u} \rho_{21}(\Delta_p', \Delta_c') e^{\frac{-v^2}{u^2}} \, dv, \tag{14}$$

where $u = \sqrt{k_B T/m}$, m is the atom's mass, k_B is Boltzmann constant, and T is the thermodynamic temperature. At normal temperature, $T = 290$ K. Due to the atomic thermal motion, the probe and coupling light detuning Δ_p' Δ_c' should be modified by the following:

$$\Delta_p' = \Delta_p - \frac{2\pi}{\lambda_p} v,$$
$$\Delta_c' = \Delta_c + \frac{2\pi}{\lambda_c} v. \tag{15}$$

Similar to the calculation method of the cold atomic model, the curves of $\Omega_{1\text{dB}}$, Ω_{min} and LDR vs Ω_p can be calculated under the condition of $\Omega_{\text{LO}} = \Omega_{\text{opt}}$. The curve of $\Omega_{1\,\text{dB}}$ vs Ω_p in the Rydberg atomic superheterodyne receiving system is shown by the solid blue line in Fig. 5(c). Compared with the case of the cold atomic model, $\Omega_{1\text{dB}}$ also increases with Ω_p. Due to the spectral broadening caused by atomic thermal motion, the value of $\Omega_{1\text{dB}}$ is uplifted. On the other hand, with the same range of P_{nf} in the cold atom model, the relationship of Ω_{min} between Ω_p can be obtained, as shown by the red shaded
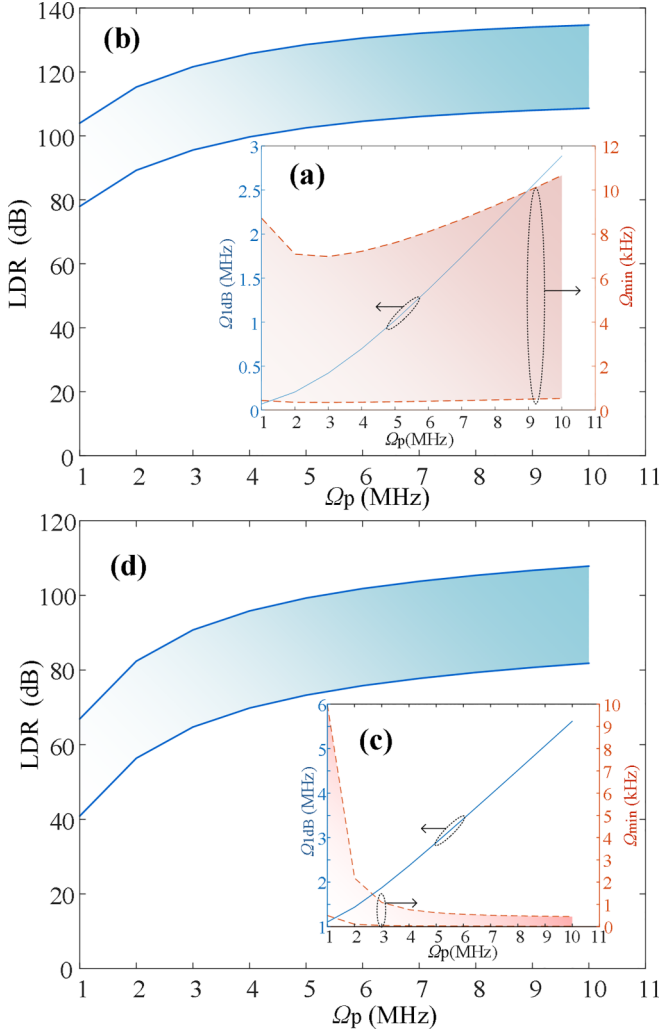
FIG. 5. The LDR vs Ω_p in (a) cold atomic model and (c) thermal atomic model; 1 dB compression point Ω_{1dB} and minimum detectable MSUT Rabi frequency Ω_{min} vs Ω_p in (b) cold atomic model and (d) thermal atomic model.
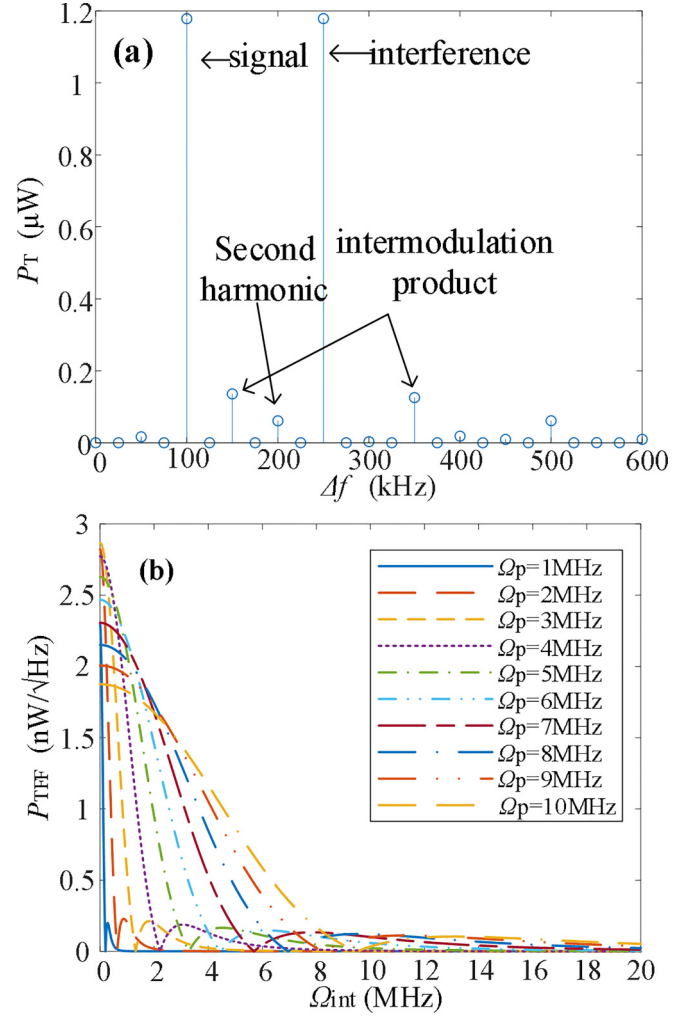

FIG. 6. (a) Spectrum of P_T with interference, where $d = 0.76$ mm, $\Omega_{LO} = \Omega_{opt}$, $\Omega_p = 6$ MHz, $\Omega_{int} = \Omega_s = 500$ kHz $\ll \Omega_{opt}$, $\Delta f_1 = 100$ kHz, $\Delta f_2 = 250$ kHz; (b) P_{TFF} vs Ω_{int} under different Ω_p when $\Omega_s = 1$ kHz.

area in Fig. 5(c), quite different from that in cold atomic model conditions. In the thermal atomic model, with the increase of Ω_p, the profile height of the EIT peak increases, and the power broadening caused by the increase of Ω_p is weakened by Doppler broadening, making $|\kappa|_{max}$ monotonically increase with Ω_p in a larger range. Due to the spectrum broadening in the thermal atomic model, which is more obvious than in the cold atomic model, there is a difference of $|\kappa|_{max}$ between the thermal and cold atomic models, and Ω_{min} increased as a whole.

Further, the relationship between LDR and Ω_p can be obtained according to $(\Omega_{1dB}/\Omega_{min})^2$, as shown by the blue shaded area in Fig. 5(d). Similar to the case of the cold atomic model, with the increase of Ω_p, the LDR increases at a faster rate at first and then slows.

In summary, the cold Rydberg atoms have a higher LDR due to better sensitivity than in the thermal atomic model with the same parameters. Better LDR can be obtained by increasing Ω_p in a proper range in both models. In the case

of poor noise performance, the LDR can exceed 80 dB by optimizing system parameters.

IV. ANTIBLOCKING PERFORMANCE OF THE RYDBERG ATOMIC SUPERHETERODYNE RECEIVER

In most application scenarios, spatial interference is unavoidable. The antiblocking performance of the Rydberg atomic superheterodyne receiving system under different Ω_p is studied in this section. A spatial interference is introduced to evaluate the antiblocking performance, which usually has a certain bandwidth. However, in the steady-state analysis model, the Rydberg atom has no selectivity for the interference frequency. For simplicity, an undesired single-frequency signal can be used as interference and act on the Rydberg atom. An interference electric field E_{int} has an amplitude of A_{int}, in which the frequency and phase difference with microwave LO signal is $\Delta f_2 (\Delta f_2 \neq \Delta f_1)$, $\Delta \varphi_2$, respectively. The interference electric field E_{int} can be expressed as

$$E_{int} = A_{int} \cos[2\pi f_{LO}(f_{LO} - \Delta f_2)t + \varphi_{LO} - \Delta \varphi_2]. \quad (16)$$
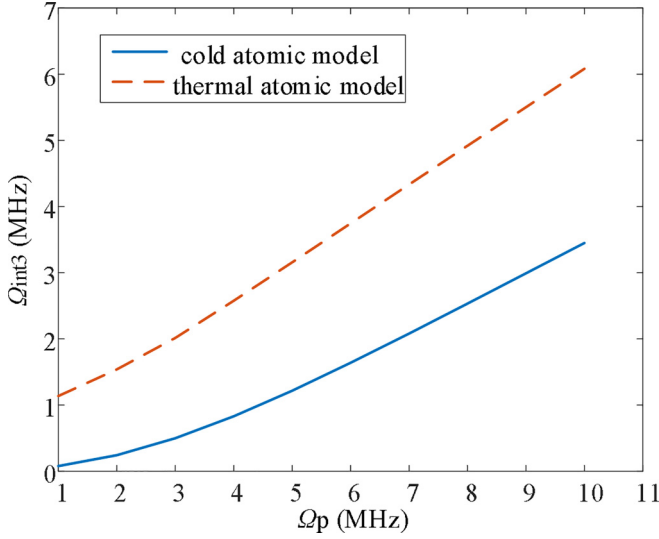
FIG. 7. Ω_{int3} vs Ω_p under the cold and thermal atomic model.

Add (16) to (6), and the envelope term E_{m} of E_{MW} can be described as

$$
\begin{aligned}
E_{\text{m}} = \{ & A_{\text{LO}}{}^2 + A_{\text{s}}{}^2 + A_{\text{int}}{}^2 \\
& + 2A_{\text{LO}}A_{\text{s}} \cos(2\pi \Delta f_1 t + \Delta\varphi_1) \\
& + 2A_{\text{LO}}A_{\text{int}} \cos(2\pi \Delta f_2 t + \Delta\varphi_2) \\
& + 2A_{\text{s}}A_{\text{int}} \cos[2\pi (\Delta f_1 - \Delta f_2)t + \Delta\varphi_1 - \Delta\varphi_2]\}^{\frac{1}{2}}.
\end{aligned}
\tag{17}
$$

The relation between P_{T} and t can be obtained by combining with (16), (1), (2), and (3), and the influence of E_{int} on VIFS can be analyzed from the spectrum of P_{T}. Set $d = 0.76$ mm, $\Omega_{\text{LO}} = \Omega_{\text{opt}}$, $\Omega_p = 6$ MHz, $\Omega_{\text{int}} = \Omega_{\text{s}} = 500$ kHz $\ll \Omega_{\text{opt}}$, $\Delta f_1 = 100$ kHz, and $\Delta f_2 = 250$ kHz, and keep other system parameters unchanged. Without considering the instantaneous bandwidth of the Rydberg atom, the spectrum results of P_{T} (filtered DC component) are shown in Fig. 6(a) in the cold atom model. In addition to P_{TFF} and its harmonic components $n\Delta f_1$ ($n = 2, 3, 4, \ldots$), the spectrum

exhibits undesired IF components caused by the interference, which includes $n\Delta f_2$, $n\Delta f_2 + \Delta f_1$, and $n\Delta f_2 - \Delta f_1$ ($n = 1, 2, 3, \ldots$), where Δf_2 has the most significant impact.

Besides distorting the signal, in most cases, strong interference in free space can block the signal reception by affecting the value of Ω_{DC}. In the cold atomic model, set $\Omega_{\text{s}} = 1$ kHz, varying Ω_{int} while keeping the other parameters unchanged. The relationship curves of P_{TFF} vs Ω_{int} under different Ω_p can be obtained, as shown in Fig. 6(b). With the increase of Ω_{int}, P_{TFF} decreases gradually, and the decreasing speed slows with the increase of Ω_p. The solid blue line in Fig. 7 shows the variation of Ω_{int3} with Ω_p in the cold atomic model, where Ω_{int3} corresponds to Ω_{int} when P_{TFF} decreases $\sqrt{2}$ times as $P_{\text{TFF}}|_{\Omega_{\text{int}}=0}$. With the increase of Ω_p, the value of Ω_{int3} gradually increases, which means that the interference strength needs to be enhanced to get the same suppression effect for the VIFS. Therefore, the Rydberg atom's antiblocking performance can be improved by increasing Ω_p. Ω_{int3} can be used as a parameter to evaluate the antiblocking performance of the system. In the thermal atomic model, with the same value of Ω_p, Ω_{int3} has a greater value than in the cold atomic model, shown as the dashed red line in Fig. 7. Thus, the system has better antiblocking performance in the thermal atomic model, which can be improved by increasing Ω_p in an acceptable range.

V. CONCLUSION

In summary, the LDR, the antiblocking performance, and ALEC can be adjusted by controlling the laser Rabi frequency. The cold atomic model has a larger LDR than the thermal atomic model due to higher sensitivity than the thermal atomic model. But the thermal atomic model has a larger 1 dB compression point and better antiblocking performance. Using a larger probe light Rabi frequency in a proper range is conducive to improving the LDR and antiblocking performance. In case of poor noise performance, the LDR can exceed 80 dB by optimizing system parameters to meet certain applications.

APPENDIX

The derivation process of (6) is as follows:

$$
\begin{aligned}
E_{\text{MW}} &= E_{\text{LO}} + E_{\text{s}} \\
&= A_{\text{LO}} \cos(2\pi f_{\text{LO}} t + \varphi_{\text{LO}}) + A_{\text{s}} \cos[2\pi f_{\text{LO}}(f_{\text{LO}} - \Delta f)t + \varphi_{\text{LO}} - \Delta\varphi] \\
&= \text{Re}[(A_{\text{LO}} + A_{\text{s}} e^{-j(2\pi \Delta f t + \Delta\varphi)}) e^{j(2\pi f_{\text{LO}} t + \varphi_{\text{LO}})}] \\
&= \text{Re}[(A_{\text{LO}} + A_{\text{s}} e^{-j(2\pi \Delta f t + \Delta\varphi)}) \cos(2\pi f_{\text{LO}} t + \varphi_{\text{LO}}) + \text{j}(A_{\text{LO}} + A_{\text{s}} e^{-j(2\pi \Delta f t + \Delta\varphi)}) \sin(2\pi f_{\text{LO}} t + \varphi_{\text{LO}})] \\
&= |A_{\text{LO}} + A_{\text{s}} e^{-j(2\pi \Delta f t + \Delta\varphi)}| \cos(2\pi f_{\text{LO}} t + \varphi_{\text{LO}}) \\
&= |A_{\text{LO}} + A_{\text{s}} \cos(2\pi \Delta f t + \Delta\varphi) + jA_{\text{LO}} \sin(2\pi \Delta f t + \Delta\varphi)| \cos(2\pi f_{\text{LO}} t + \varphi_{\text{LO}}) \\
&= \cos(2\pi f_{\text{LO}} t + \varphi_{\text{LO}}) \sqrt{A_{\text{LO}}^2 + A_{\text{s}}^2 + 2A_{\text{LO}}A_{\text{s}} \cos(2\pi \Delta f t + \Delta\varphi)} \\
&= E_m \times E_c,
\end{aligned}
\tag{A1}
$$

where carrier term E_{c} is

$$
E_{\text{c}} = \cos(2\pi f_{\text{LO}} t + \varphi_{\text{LO}})
\tag{A2}
$$

and the Envelope term E_m is

$$E_m = \sqrt{A_{LO}^2 + A_s^2 + 2A_{LO}A_s \cos(2\pi \Delta f t + \Delta\varphi)}. \tag{A3}$$

Let $x = A_s/A_{LO}$, and through Taylor series expansion of E_c at $x = 0$, (6) can be obtained.

[1] D. A. Anderson, R. E. Sapiro, and G. Raithel, An atomic receiver for AM and FM radio communication, IEEE Trans. Antennas Propag. **69**, 2455 (2020).

[2] C. Holloway, M. Simons, A. H. Haddab, J. A. Gordon, D. A. Anderson, G. Raithel, and S. Voran, A multiple-band Rydberg atom-based receiver: AM/FM stereo reception, IEEE Antennas Propag. Mag. **63**, 63 (2020).

[3] Z. Song, H. Liu, X. Liu, W. Zhang, H. Zou, J. Zhang, and J. Qu, Rydberg-atom-based digital communication using a continuously tunable radio-frequency carrier, Opt. Express **27**, 8848 (2019).

[4] C. L. Holloway, M. T. Simons, A. H. Haddab, C. J. Williams, and M. W. Holloway, A "real-time" guitar recording using Rydberg atoms and electromagnetically induced transparency: Quantum physics meets music, AIP Adv. **9**, 065110 (2019).

[5] M. T. Simons, A. H. Haddab, J. A. Gordon, D. Novotny, and C. L. Holloway, Embedding a Rydberg atom-based sensor into an antenna for phase and amplitude detection of radio-frequency fields and modulated signals, IEEE Access **7**, 164975 (2019).

[6] C. L. Holloway, M. T. Simons, J. A. Gordon, and D. Novotny, Detecting and receiving phase-modulated signals with a Rydberg atom-based receiver, Antennas Wirel. Propag. Lett. **18**, 1853 (2019).

[7] D. H. Meyer, P. D. Kunz, and K. C. Cox, Waveguide-Coupled Rydberg Spectrum Analyzer from 0 to 20 GHz, Phys. Rev. Appl. **15**, 014053 (2021).

[8] A. K. Robinson, N. Prajapati, D. Senic, M. T. Simons, and C. L. Holloway, Determining the angle-of-arrival of a radio-frequency source with a Rydberg atom-based sensor, Appl. Phys. Lett. **118**, 114001 (2021).

[9] F. Wu, Y. Lin, B. Wu, and Y. Fu, Response characteristics of radio frequency pulse of Rydberg atoms, Acta Phys. Sin. **71**, 207402 (2022).

[10] M. T. Simons, J. A. Gordon, and C. L. Holloway, Fiber-coupled vapor cell for a portable Rydberg atom-based radio frequency electric field sensor, Appl. Opt. **57**, 6456 (2018).

[11] K. C. Cox, D. H. Meyer, F. K. Fatemi, and P. D. Kunz, Quantum-Limited Atomic Receiver in the Electrically Small Regime, Phys. Rev. Lett. **121**, 110502 (2018).

[12] R. Mao, Y. Lin, K. Yang, Q. An, and Y. Fu, A high-efficiency fiber-coupled Rydberg-atom integrated probe and its imaging applications, IEEE Antennas Wireless Propag. Lett. **22**, 352 (2023).

[13] L. Yi, W. Feng-Chuan, M. Rui-Qi, Y. Jia-Wei, L. Yi, A. Qiang, and F. Yun-Qi, Development of three-port fiber-coupled vapor cell probe and its application in microwave digital communication, Acta Phys. Sin. **71**, 170702 (2022).

[14] L. J. Chu, Physical limitations of omni-directional antennas, J. Appl. Phys. **19**, 1163 (1948).

[15] R. F. Harrington, Effect of antenna size on gain, bandwidth, and efficiency, J. Res. Natl. Bur. Stand. Sect. D **64** (1960).

[16] C. L. Holloway, J. A. Gordon, S. Jefferts, A. Schwarzkopf, D. A. Anderson, S. A. Miller, N. Thaicharoen, and G. Raithel, Broadband Rydberg atom-based electric-field probe for SI-traceable, self-calibrated measurements, IEEE Trans. Antennas Propag. **62**, 6169 (2014).

[17] K. Yang, Q. An, J. Yao, R. Mao, Y. Lin, Y. Liu, and Y. Fu, Rydberg atom-based ultra-broadband radio frequency sensor from 100 kHz to 40 GHz, Acta Opt. Sin. **42**, 1528002 (2022).

[18] N. Thaicharoen, K. R. Moore, D. A. Anderson, R. C. Powel, E. Peterson, and G. Raithel, Electromagnetically induced transparency, absorption, and microwave-field sensing in a Rb vapor cell with a three-color all-infrared laser system, Phys. Rev. A **100**, 063427 (2019).

[19] J. Shaffer and H. Kübler, A read-out enhancement for microwave electric field sensing with Rydberg atoms, in *Proceedings of the 2018 Quantum Technologies Conference*, Strasbourg, France, 2018 (SPIE, Bellingham, 2018).

[20] J. S. Cabral, J. M. Kondo, L. F. Gonçalves, L. G. Marcassa, D. Booth, J. Tallant, and J. P. Shaffer, Manipulation of quantum state transfer in cold Rydberg atom collisions, New J. Phys. **12**, 093023 (2010).

[21] S. Kumar, H. Fan, H. Kübler, J. Sheng, and J. P. Shaffer, Atom-based sensing of weak radio frequency electric fields using homodyne readout, Sci. Rep. **7**, 42981 (2017).

[22] M. T. Simons, J. A. Gordon, C. L. Holloway, D. A. Anderson, S. A. Miller, and G. Raithel, Using frequency detuning to improve the sensitivity of electric field measurements via electromagnetically induced transparency and Autler-Townes splitting in Rydberg atoms, Appl. Phys. Lett. **108**, 174101 (2016).

[23] S. Kumar, H. Fan, H. Kübler, A. J. Jahangiri, and J. P. Shaffer, Rydberg-atom based radio-frequency electrometry using frequency modulation spectroscopy in room temperature vapor cells, Opt. Express **25**, 8625 (2017).

[24] M. Cai, Z. Xu, S. You, and H. Liu, Sensitivity improvement and determination of Rydberg atom-based microwave sensor, Photon. **9**, 250 (2022).

[25] M. Jing, Y. Hu, J. Ma, H. Zhang, L. Zhang, L. Xiao, and S. Jia, Atomic superheterodyne receiver based on microwave-dressed Rydberg spectroscopy, Nat. Phys. **16**, 911 (2020).

[26] N. Prajapati, A. K. Robinson, S. Berweger, M. T. Simons, A. B. Artusio-Glimpse, and C. L. Holloway, Enhancement of electromagnetically induced transparency based Rydberg-atom electrometry through population repumping, Appl. Phys. Lett. **119**, 214001 (2021).

[27] C. L. Holloway, M. T. Simons, J. A. Gordon, P. F. Wilson, C. M. Cooke, D. A. Anderson, and G. Raithel, Atom-based RF

electric field metrology: From self-calibrated measurements to subwavelength and near-field imaging, IEEE Trans. Electromag. Compat. **59**, 717 (2017).

[28] H. Fan, S. Kumar, J. Sheng, J. P. Shaffer, C. L. Holloway, and J. A. Gordon, Effect of Vapor-Cell Geometry on Rydberg-Atom-Based Measurements of Radio-Frequency Electric Fields, Phys. Rev. Appl. **4**, 044015 (2015).

[29] B. Wu, Y. Lin, D. Liao, Y. Liu, Q. An, and Y. Fu, Design of locally enhanced electric field in dielectric loaded rectangular resonator for quantum microwave measurements, Electron. Lett. **58**, 914 (2022).

[30] D. Anderson, E. Paradis, and G. Raithel, A vapor-cell atomic sensor for radio-frequency field detection using a polarization-selective field enhancement resonator, Appl. Phys. Lett. **113**, 073501 (2018).

[31] C. L. Holloway, N. Prajapati, A. B. Artusio-Glimpse, S. Berweger, M. T. Simons, Y. Kasahara, A. Alù, and R. W. Ziolkowski, Rydberg atom-based field sensing enhancement using a split-ring resonator, Appl. Phys. Lett. **120**, 204001 (2022).

[32] J. A. Gordon, M. T. Simons, A. H. Haddab, and C. L. Holloway, Weak electric-field detection with sub-1 Hz resolution at radio frequencies using a Rydberg atom-based mixer, AIP Adv. **9**, 045030 (2019).

[33] C. T. Fancher, D. R. Scherer, M. C. S. John, and B. L. S. Marlow, Rydberg atom electric field sensors for communications and sensing, IEEE Trans. Quantum Eng. **2**, 1 (2021).

[34] J. A. Sedlacek, A. Schwettmann, H. Kübler, and J. P. Shaffer, Atom-Based Vector Microwave Electrometry Using Rubidium

Rydberg Atoms in a Vapor Cell, Phys. Rev. Lett. **111**, 063001 (2013).

[35] J. A. Sedlacek, A. Schwettmann, H. Kübler, R. Löw, T. Pfau, and J. P. Shaffer, Microwave electrometry with Rydberg atoms in a vapour cell using bright atomic resonances, Nat. Phys. **8**, 819 (2012).

[36] H. Fan, S. Kumar, J. Sedlacek, H. Kübler, S. Karimkashi, and J. P. Shaffer, Atom based RF electric field sensing, J. Phys. B: At. Mol. Opt. Phys. **48**, 202001 (2015).

[37] C. L. Holloway, M. T. Simons, J. A. Gordon, A. Dienstfrey, D. A. Anderson, and G. Raithel, Electric field metrology for SI traceability: Systematic measurement uncertainties in electromagnetically induced transparency in atomic vapor, J. Appl. Phys. **121**, 233106 (2017).

[38] D. A. Anderson, R. E. Sapiro, and G. Raithel, A self-calibrated SI-traceable Rydberg atom-based radio frequency electric field probe and measurement instrument, IEEE Trans. Antennas Propag. **69**, 5931 (2021).

[39] M. T. Simons, A. H. Haddab, J. A. Gordon, and C. L. Holloway, A Rydberg atom-based mixer: Measuring the phase of a radio frequency wave, Appl. Phys. Lett. **114**, 114101 (2019).

[40] M. G. Bason, M. Tanasittikosol, A. Sargsyan, A. Mohapatra, D. Sarkisyan, R. Potvliege, and C. Adams, Enhanced electric field sensitivity of RF-dressed Rydberg dark states, New J. Phys. **12**, 065015 (2010).

[41] F. Wu, Q. An, Z. Sun, and Y. Fu, Research on intrinsic expansion coefficients in Rydberg atomic heterodyne receiving link, Acta Phys. Sin. **72**, 047401 (2023).